The Journal of Physiology

Exploring the role of the Kölliker–Fuse nucleus in breathing variability by mathematical modelling

S. R. John[1], W. H. Barnett[2], A. P. L. Abdala[3], D. B. Zoccal[4], J. E. Rubin[1] and Y. I. Molkov[5]

[1] *University of Pittsburgh, Pittsburgh, PA, USA*
[2] *Indiana University Purdue University Indianapolis, Indianapolis, IN, USA*
[3] *University of Bristol, Bristol, UK*
[4] *São Paulo State University, Araraquara, Brazil*
[5] *Georgia State University, Atlanta, GA, USA*

Handling Editors: Harold Schultz & Frank Powell

The peer review history is available in the Supporting Information section of this article (https://doi.org/10.1113/JP285158#support-information-section).

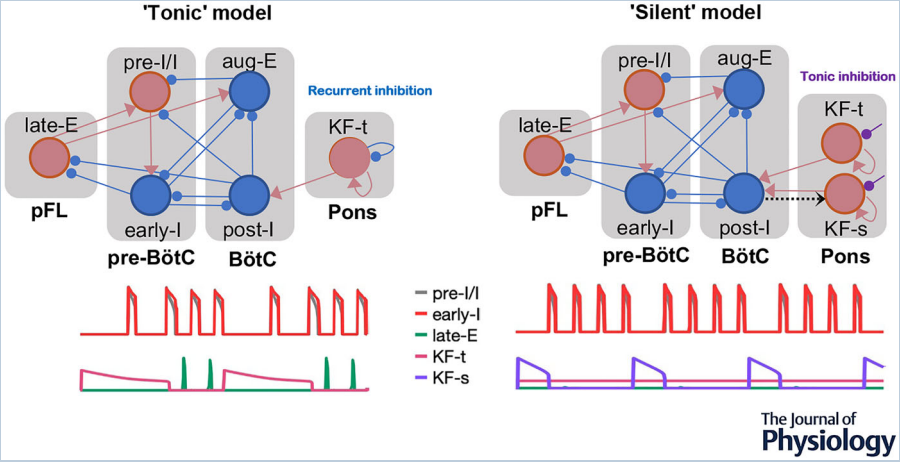

Abstract The Kölliker–Fuse nucleus (KF), which is part of the parabrachial complex, participates in the generation of eupnoea under resting conditions and the control of active abdominal expiration when increased ventilation is required. Moreover, dysfunctions in KF neuronal activity are believed to play a role in the emergence of respiratory abnormalities seen in Rett syndrome (RTT), a progressive neurodevelopmental disorder associated with an irregular breathing pattern and frequent apnoeas. Relatively little is known, however, about the intrinsic dynamics of neurons

Sushmita John graduated with a PhD in Mathematics from the University of Pittsburgh. Her research focuses on the patterning and robustness of bursting patterns exhibited by respiratory neuronal models.

S. R. John and W. H. Barnett contributed equally.
J. E. Rubin and Y. I. Molkov share senior authorship.
This article was first published as a preprint. John, S, Barnett, W, Abdala, A, Zoccal, D, Rubin, J, Molkov, Y. 2023. The role of Kölliker-Fuse nucleus in breathing variability. bioRxiv. https://doi.org/10.1101/2023.06.15.545086

 DOI: 10.1113/JP285158

within the KF and how their synaptic connections affect breathing pattern control and contribute to breathing irregularities. In this study, we use a reduced computational model to consider several dynamical regimes of KF activity paired with different input sources to determine which combinations are compatible with known experimental observations. We further build on these findings to identify possible interactions between the KF and other components of the respiratory neural circuitry. Specifically, we present two models that both simulate eupnoeic as well as RTT-like breathing phenotypes. Using nullcline analysis, we identify the types of inhibitory inputs to the KF leading to RTT-like respiratory patterns and suggest possible KF local circuit organizations. When the identified properties are present, the two models also exhibit quantal acceleration of late-expiratory activity, a hallmark of active expiration featuring forced exhalation, with increasing inhibition to KF, as reported experimentally. Hence, these models instantiate plausible hypotheses about possible KF dynamics and forms of local network interactions, thus providing a general framework as well as specific predictions for future experimental testing.

(Received 15 June 2023; accepted after revision 9 November 2023; first published online 6 December 2023)
Corresponding author Y. I. Molkov: Department of Mathematics and Statistics, Georgia State University, 25 Park Place, Atlanta, GA 30303, USA. Email: ymolkov@gsu.edu

Abstract figure legend Some forms of periodic breathing may be driven by slow endogenous oscillations in the activity of the Kölliker–Fuse nucleus.

Key points

- The Kölliker–Fuse nucleus (KF), a part of the parabrachial complex, is involved in regulating normal breathing and controlling active abdominal expiration during increased ventilation.
- Dysfunction in KF neuronal activity is thought to contribute to respiratory abnormalities seen in Rett syndrome (RTT). This study utilizes computational modelling to explore different dynamical regimes of KF activity and their compatibility with experimental observations.
- By analysing different model configurations, the study identifies inhibitory inputs to the KF that lead to RTT-like respiratory patterns and proposes potential KF local circuit organizations.
- Two models are presented that simulate both normal breathing and RTT-like breathing patterns.
- These models provide testable hypotheses and specific predictions for future experimental investigations, offering a general framework for understanding KF dynamics and potential network interactions.

Introduction

Breathing is an automatic process produced and shaped by the respiratory central pattern generator (rCPG), which comprises several neural structures in the brainstem (Smith et al., 2007). Extensive work has characterized the synaptic and ionic mechanisms that generate and regulate the activity of ventromedullary respiratory neurons and how these mechanisms affect breathing rhythm and pattern. This study focuses on a major counterpart to the medullary rCPG: the pontine Kölliker–Fuse nucleus (KF). The KF is part of the parabrachial complex in the dorsolateral pons and is formed by a collection of neurons surrounding the superior cerebellar peduncle (Varga et al., 2021). Although it was first described as the inspiratory off-switch centre, compelling evidence indicates that the KF activity critically contributes to maintaining the eupnoeic three-phase respiratory pattern (inspiration, post-inspiration, and stage 2 of expiration). Moreover, KF neurons are required for adjusting breathing characteristics across a range of conditions.

Much of this evidence derives from studies featuring significant perturbations in KF activity. For example, lesions of the KF substantially alter the respiratory pattern, introducing augmented variability in frequency and amplitude, or even eliminating the post-inspiratory phase and thus disrupting eupnoeic breathing (Bautista & Dutschmann, 2014a; Dutschmann & Herbert, 2006; Fung & St John, 1995; Jenkin et al., 2017; Oku & Dick, 1992; Silva et al., 2016). Chemical excitation of KF neurons enhances constrictor activity in upper airway muscles and prolongs the duration of the post-inspiratory phase of the respiratory cycle (Dutschmann & Herbert, 2006). In contrast, disruption of GABAergic

transmission in the KF induces periodic apnoeas, respiratory irregularities and the loss of abdominal expiratory contractions (or active expiration) during exposure to high levels of carbon dioxide (Abdala et al., 2016; Barnett et al., 2018; Dhingra et al., 2016). KF neurons are also targets for neuromodulators that modify neuronal excitability and change the breathing pattern and rhythm. In this regard, activating 5-HT_{1A} (serotonin) receptors in the KF reduces spontaneous apnoeas, while antagonizing these receptors can destabilize breathing frequency (Dhingra et al., 2016). Some KF neurons express μ-opioid receptors that, when activated, can cause breathing irregularities and bring about life-threatening apnoeas, a mechanism associated with opioid-induced respiratory depression (Bachmutsky et al., 2020). In addition to the control of eupnoeic breathing, the KF also contributes to the respiratory adjustments related to behaviours such as vocalization, swallowing and coughing (Bautista & Dutschmann, 2014b; Dutschmann & Dick, 2012; Jakus et al., 2008), acting as a convergent and integrative synaptic station that relays inputs from suprapontine regions to the rCPG (Hayward et al., 2004). Despite the evidence showing the critical role of the KF in breathing control, its cellular organization and interaction with other respiratory compartments to adjust the respiratory rhythm and pattern remain uncertain.

There is a long tradition of using mathematical modelling and computational techniques to build theoretical models of the rCPG, develop intuition about how it functions, and test hypotheses on respiratory rhythm and pattern generation (Lindsey et al., 2012; Molkov et al., 2017; Phillips & Rubin, 2022). In the past, we developed models integrating a medullary CPG circuit with a pontine component using an established reduced, activity-based mathematical framework (Barnett et al., 2018; Flor et al., 2020; Molkov et al., 2017; Rubin et al., 2009, 2011; Wittman et al., 2019). Previous models differed in their assumptions about pontine interactions and intrinsic dynamics, which need to be better characterized experimentally. These models have provided a proof of principle for the proposed central role of the KF in respiratory control and have yielded preliminary predictions about interactions of the KF with other pontine and medullary respiratory areas as well as their contribution to respiratory rhythmicity and pattern formation under a variety of conditions. The details of these predictions, however, depend on the assumptions made about intrinsic properties and activity patterns of KF neurons, synaptic interactions in the circuit, and conditions leading to aberrant KF activity and subsequent perturbations of breathing. To reproduce specific experimental observations, model networks that include the KF have required the presence of specific synaptic pathways, such as from inhibitory neurons in the Bötzinger complex (BötC) (Wittman et al., 2019) and nucleus tractus solitarii (NTS) pump cells (Molkov et al., 2013). Models have also suggested that KF neurons may have certain intrinsic properties modulating their activity such as endogenous bursting (Wittman et al., 2019). This capability, however, has never been demonstrated experimentally.

Understanding the mechanisms underlying the control of KF activity is essential to identify its role in breathing pattern formation in eupnoea (Smith et al., 2007) and to determine how changes in these mechanisms affect the expiratory motor pattern (Barnett et al., 2018; Koolen, 2021) and contribute to inducing stereotyped breathing patterns such as those observed in Rett syndrome (Abdala et al., 2016). The latter was previously modelled by Wittman et al. (2019) who showed that certain assumptions about the intrinsic properties of the KF neurons and patterns of connections between KF and other respiratory structures can explain the emergence of irregular breathing when inhibition in KF is compromised. However, the validity of some of the assumptions made in that work is unknown and they await experimental testing, and the authors did not compare model behaviour with experimental findings about manipulations that change the efficacy of inputs to KF neurons. Moreover, their reduced model did not include the components necessary to explore the KF's role in active expiration control. In this study, we assume only that KF provides excitatory drive to an expiratory component of the medullary respiratory network and exhibits simple (tonic spiking or silent) activity in the absence of synaptic input. We consider various hypothetical local sources for this input and assess which may explain a set of experimental observations not previously addressed. Specifically, each model configuration was tested against the following list of benchmarks based on the literature: (1) reduction of GABA/5-HT_{1A} inhibition in the KF leads to an aberrant respiratory pattern in which breathing is intermittently disrupted by periods of apnoea (Abdala et al., 2016; Dhingra et al., 2016); (2) the duration of apnoeic periods is relatively constant or increases as the inhibition level to KF decreases (Abdala et al., 2016; Dhingra et al., 2016); (3) when KF is dysfunctional, a sufficient inhibition of the KF neurons transforms intermittent breathing into eupnoea (Abdala et al., 2010, 2016); (4) a further increase in inhibition of the KF neurons alters the respiratory pattern by inducing the abdominal expiratory activity during the late part of the E2, or late-E, phase of the respiratory cycle, with a frequency that increases in a step-wise, or quantal, manner as inhibition is strengthened (Koolen, 2021). We discuss two viable model configurations, while presenting evidence against certain others, and formulate experimentally testable implications in each case.

Methods

To study the contribution of KF activity to the generation and modulation of various respiratory patterns, we developed and analysed two families of computational models of a respiratory brain stem neuronal circuit. In the first family, which we call the *tonic model*, the KF population is homogeneous with steady, sustained or *tonic* activity under normal conditions. The other family combines two KF populations, one that shows sustained tonic activity (as in the tonic model) and another that is intrinsically silent under normal conditions. Based on the inclusion of the second population, we refer to this as the *silent model*. Schematic diagrams of the models are shown in Fig. 1.

The models presented in this work are adapted from previous models for respiratory neurons and circuits (Rubin et al., 2009, 2011; Wittman et al., 2019). To form these models, we incorporated the KF component into a pre-existing model presented by Rubin et al. (2011). Similarly, to that model, the models in this work include the following respiratory populations, which together comprise what we call the *respiratory core*: pre-inspiratory (pre-I) and early-inspiratory (early-I) populations of the pre-Bötzinger complex (pre-BötC) and post-inspiratory (post-I) and augmenting expiratory (aug-E) populations of the Bötzinger complex (BötC). The pre-I and early-I populations are active during the inspiratory phase of respiration (I phase), whereas aug-E and post-I are active during the expiratory phase (E phase). More precisely, post-I units feature a surge of activity at the onset of expiration, followed by a gradual tailing off of activity. In contrast, aug-E units gradually ramp up their activity, in an augmenting pattern, over the course of expiration. The models also include a late-expiratory (late-E) population of the lateral parafacial region (pFL), which remains inactive during resting breathing (Bianchi et al., 1995).

All of the synaptic connections between these respiratory populations in the models shown in Fig. 1 are either directly shown in, or inferred from, experimental observations (Molkov et al., 2010; Rubin et al., 2011). Both models also include a KF sub-population, named KF-t, that is tonically active under normal conditions and helps to maintain eupnoea. The silent model includes KF-t and another KF sub-population, named KF-s, that is silent under normal conditions. The interactions of the KF units with the respiratory core in these models occur through excitatory connections from KF-t and KF-s to the post-I population. These connections have been proposed previously (Barnett et al., 2018; Geerling et al., 2017; Jenkin et al., 2017; Molkov et al., 2013). Little is known about sources of inhibition to KF neurons. For exploratory purposes, we considered both tonic inhibition to the KF originating from an unspecified outside source and recurrent inhibitory connections within the KF. We analyse the extent to which each of these inhibition types, within each model, yields outputs consistent with respiratory perturbations seen in Rett syndrome (RTT), and we also study the emergence of late-E activity (active expiration). Previous work by Wittman et al. (2019) introduced a simplified representation of pulmonary stretch receptor feedback related to I phase output. As part of the analysis of the silent model done in the current paper, we study the primary effect of this pathway by considering what happens if we introduce an additional excitatory connection from post-I to KF-s (shown as a black dashed arrow in Fig. 1*B*). Although this connection would need to run through another inhibitory population and thus be manifested via disynaptic disinhibition in reality, for simplicity we treat it as a monosynaptic excitation in this work.

Each component in these models is described by a single two-dimensional system of Hodgkin–Huxley type equations representing the dynamics of a membrane

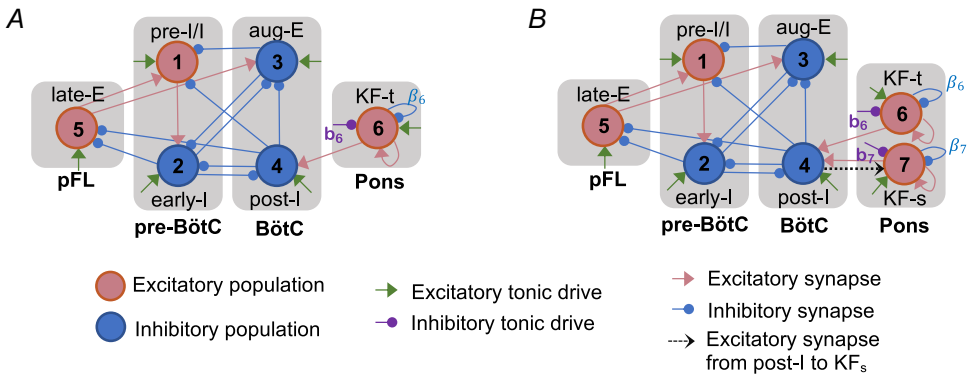

Figure 1. Schematic diagrams for the respiratory network models considered in this work
A, tonic model; *B*, silent model. The labels b_6, b_7, β_6 and β_7 refer to parameters used to represent the strengths of certain connections explored in the model. Abbreviations referring to neuronal populations and sites are described in the text. [Colour figure can be viewed at wileyonlinelibrary.com]

voltage variable v and a secondary slow variable h or m. We consider this framework as a simplified representation of dynamics in which the activity levels of neurons within each population are synchronized, and the reduction that it provides allows us to use the tools of phase plane analysis to understand model dynamics and the effects of parameter variations. To present the equations for this system, we assign a subscript from 1 to 5 for the pre-I/I, early-I, aug-E, post-I and late-E units, respectively. The KF-t unit is labelled as 6 and the additional KF-s unit in the silent models as 7.

The pre-I/I ($i = 1$) and late-E ($i = 5$) units feature a persistent sodium current (Butera et al., 1999; Molkov et al., 2010; Rubin et al., 2011) and hence are represented by the following differential equations:

$$\begin{aligned} v_i^{'} &= (I_{\mathrm{NaP}_i} + I_{\mathrm{K}_i} + I_{\mathrm{L}_i} + I_{\mathrm{syne}_i} + I_{\mathrm{syni}_i} + \sigma W_i)/C \\ h_i' &= \left(h_{\mathrm{NaP}}\left(v_i\right) - h_i\right)/t_{\mathrm{NaP}}\left(v_i\right) \end{aligned} \tag{1}$$

where C is the membrane capacitance, I_{NaP_i} is the persistent sodium current, I_{K_i} represents the delayed rectifier potassium current, I_{L_i} is the leak current, I_{syne_i} and I_{syni_i} are the excitatory and inhibitory synaptic currents, and W_i are independent random processes representing the noise with the magnitude regulated by parameter σ, for each unit.

All of the other units in the model network $i \in \{2, 3, 4, 6, 7\}$ are modelled as adapting neurons and obey the following equations:

$$\begin{aligned} v_i' &= (I_{\mathrm{AD}_i} + I_{\mathrm{K}_i} + I_{\mathrm{L}_i} + I_{\mathrm{syne}_i} + I_{\mathrm{syni}_i} + \sigma W_i)/C \\ m_i' &= (\gamma_i f_i\ (v_i) - m_i)/t_{\mathrm{AD}} \text{ for } i \in \{2,\ 3,\ 4\} \\ m_i' &= p_i\left(\alpha_i f_i\left(v_i\right) - m_i\right)/t_{\mathrm{AD}_i} \text{ for } i \in \{6,\ 7\} \end{aligned} \tag{2}$$

where I_{AD_i} is a second potassium current causing adaptation during spiking and t_{AD} is a constant shared for all $i \in \{2, 3, 4\}$. Importantly, the function $t_{\mathrm{NaP}}\ (v)$ from Equation (1) and parameter t_{AD} and t_{AD_i} from Equation (2) are small relative to the time scale of the voltage variables, such that the h_i and m_i evolve relatively slowly.

The various currents in Equations (1) and (2) are defined as follows:

$$\begin{aligned} I_{\mathrm{NaP}_i} &= g_{\mathrm{NaP}_i} \times m_{\mathrm{NaP}}\left(v_i\right) \times h_i \times \left(v_i - e_{\mathrm{Na}}\right) \\ I_{\mathrm{K}_i} &= g_{\mathrm{K}_i} \times m_{\mathrm{K}}^4\left(v_i\right) \times \left(v_i - e_{\mathrm{K}_i}\right) \\ I_{\mathrm{AD}_i} &= g_{\mathrm{AD}} \times m_i \times \left(v_i - e_{\mathrm{K}_i}\right) \\ I_{\mathrm{L}_i} &= g_{\mathrm{L}_i} \times \left(v_i - e_{\mathrm{L}_i}\right) \\ I_{\mathrm{syne}_i} &= g_{\mathrm{syne}} \times \left(v_i - e_{\mathrm{syne}}\right)\left(\alpha_i f_i\left(v_i\right) + a_i \right. \\ &\qquad \left. + \sum_{j\,=\,1,\,j\neq i}^{7} a_{i,\,j} f_j\left(v_j\right)\right) \\ I_{\mathrm{syni}_i} &= g_{\mathrm{syni}} \times \left(v_i - e_{\mathrm{syni}}\right)\left(\beta_i f_i\left(v_i\right) + b_i \right. \\ &\qquad \left. + \sum_{j\,=\,1,\,j\neq i}^{7} b_{i,\,j} f_j\left(v_j\right)\right) \end{aligned} \tag{3}$$

The noise term, σW_i, in Equations (1) and (2) is implemented numerically by adding the quantity $\sigma\sqrt{dt} \times w_i$ to the right-hand side of each equation, where w_i is sampled from the standard normal distribution on each time step dt. For most of the analysis in this work, we turn off the noise by setting $\sigma = 0$. We indicate clearly where noise has been turned on when we describe the results.

Inclusion of the noise term is intended to assess the robustness of the model and may represent the effects of transmembrane current fluctuations arising due to factors, such as random variations in synaptic inputs and stochastic membrane channel kinetics, that are not explicitly modelled.

The activation functions associated with Equations (1)–(3) are given by:

$$\begin{aligned} m_{\mathrm{NaP}}\ \left(v_i\right) &= \left(1 + \exp\left(\frac{v_i - v_{m\mathrm{NaP}}}{k_{m\mathrm{NaP}}}\right)\right)^{-1} \\ h_{\mathrm{NaP}}\left(v_i\right) &= \left(1 + \exp\left(\frac{v_i - v_{h\mathrm{NaP}}}{k_{h\mathrm{NaP}}}\right)\right)^{-1} \\ m_{\mathrm{K}}\ \left(v_i\right) &= \left(1 + \exp\left(\frac{v_i - v_{m\mathrm{K}}}{k_{m\mathrm{K}}}\right)\right)^{-1} \\ t_{\mathrm{NaP}}\left(v_i\right) &= t_{\mathrm{NaP}}\left(\cosh\left(\frac{v_i - v_{h\mathrm{NaP}}}{k_{h\mathrm{NaP}}}\right)\right)^{-1} \\ t_{\mathrm{AD}_i} &= c_i + n_i\left(1 + \cosh\left(\frac{v_i - v_{\mathrm{AD}_i}}{k_{\mathrm{AD}_i}}\right)\right)^{-1} \end{aligned} \tag{4}$$

with the constants c_i, n_i defined for $i \in \{6, 7\}$. The *output function* f_i for $i \in \{1, 2, 3, 4, 5\}$, which appears in both Equations (2) and (3), takes the piecewise linear form

$$f_i\left(v_i\right) = \begin{cases} 0 & \text{if } v_i \leq v_{\min} \\ \frac{v_i - v_{\min}}{v_{\max} - v_{\min}} & \text{if } v_{\min} < v_i < v_{\max} \\ 1 & \text{if } v_i \geq v_{\max} \end{cases} \tag{5}$$

whereas the output function f_i for $i \in \{6, 7\}$ is given by

$$f_i\left(v_i\right) = \begin{cases} 0 & \text{if } v_i \leq v_{\min} \\ \frac{v_i - v_{\min}}{-v_{\min}} & \text{if } v_i > v_{\min} \end{cases} \tag{6}$$

for constants $v_{\max}$ and $v_{\min}$.

The default values of these constants and all other parameters used in the models appear in Tables 1 and 2. The models were implemented using the XPPAUT software package (Ermentrout, 2002). The data obtained from the simulations performed in XPPAUT was used in MATLAB (R2022a; The MathWorks, Natick, MA,

Table 1. Default parameter values for the tonic model

$g_{NaP_i} = 5.0$ nS ($i \neq 5$)	$g_{NaP_5} = 4.72$ nS	$g_{K_i} = 5$ nS ($i \neq 6$)	$g_{K_6} = 0.0$ nS
$g_{L_i} = 2.8$ nS ($i \neq 6$)	$g_{L_6} = 2.5$ nS	$g_{AD} = 10.0$ nS	$g_{syne} = 10.0$ nS
$g_{syni} = 60.0$ nS	$e_{Na} = 50.0$ mV	$e_{K_i} = -85.0$ mV ($i \neq 6$)	$e_{K_6} = -90.0$ mV
$e_{L_i} = -60.0$ mV ($i \neq 6$)	$e_{L_6} = -66.5$ mV	$e_{syne} = 0.0$ mV	$e_{syni} = -75.0$ mV
$a_1 = 0.03$	$a_2 = 0.875$	$a_3 = 0.9$	$a_4 = 0.6$
$a_5 = 0.11$	$a_6 = 0.15$	$a_{12} = 0.5$	$a_{51} = 0.5$
$a_{53} = 0.25$	$a_{64} = 0.95$	$\alpha_6 = 1.0$	$b_6 = 0.001$
$b_{23} = 0.42$	$b_{24} = 0.22$	$b_{25} = 0.09$	$b_{31} = 0.15$
$b_{32} = 0.1$	$b_{41} = 1.0$	$b_{42} = 0.66$	$b_{43} = 0.2$
$b_{45} = 0.101$	$\beta_6 = 0.05$	$t_{NaP} = 4.0 \times 10^3$	$t_{AD} = 2.0 \times 10^3$
$v_{mNaP} = -40.0$ mV	$v_{mK} = -30.0$ mV	$v_{hNaP} = -55.0$ mV	$v_{max} = -20.0$ mV
$k_{mNaP} = -6.0$ mV	$k_{mK} = -4.0$ mV	$k_{hNaP} = 10.0$ mV	$v_{min} = -50.0$ mV
$c_6 = 7.0 \times 10^2$	$n_6 = 1.0 \times 10^4$	$v_{AD_6} = -42.0$ mV	$k_{AD_6} = 0.9$ mV
$\gamma_i = 1.0$ ($i \neq 4$)	$\gamma_4 = 2.0$	$\sigma = 0.0$	$p_6 = 0.0286$

Table 2. Default parameter values for the silent model

$a_7 = 0.1$	$a_{74} = 0.75$	$\alpha_7 = 1.0$	$\beta_7 = 0.0$
$n_7 = 5.0 \times 10^3$	$v_{AD_7} = -50$ mV	$k_{AD_7} = -0.5$ mV	$p_7 = 0.02$
$b_7 = 0.02$	$c_7 = 4.0 \times 10^2$		

The other parameter values for the model are as given in Table 1.

USA) to generate most of the figures. All the simulations were performed on a standard laptop computer (macOS, 1.4 GHz Quad-Core Intel Core i5 Processor, 8 GB RAM).

Results

Tonic model

Transitions from normal breathing to periodic breathing. For the default parameter values given in Table 1, the tonic model generates a eupnoeic breathing pattern (Fig. 2*A*). Notice that KF-t is assumed to exhibit tonic activity, with a constant non-zero output $f_6(v_6) \approx 0.15$ (pink), which may result from sustained drive from elsewhere in the pons that may potentially be tuned by feedback pathways. The tonic excitatory input from KF-t promotes the long E phase duration compared to the I phase duration during normal breathing activity in the model. Experiments show that a significant reduction of the GABA inhibition to the KF leads to respiratory apnoeas (Abdala et al., 2016), suggesting the hypothesis that such a reduction underlies respiratory disruptions as seen in RTT. When the level of sustained inhibition to KF-t in the model is reduced, KF-t produces endogenous oscillations, which in turn lead to a prolonged active phase of the post-I population on some cycles that interrupt the normal breathing pattern and would manifest as respiratory apnoeas in a physiological system (Fig. 2*B*). A comparison of the KF-t output traces between the two panels of Fig. 2 shows that while KF-t output is elevated during the active phase of its oscillations relative to its sustained output level in the tonic case, the KF-t output becomes lower than the tonic level during

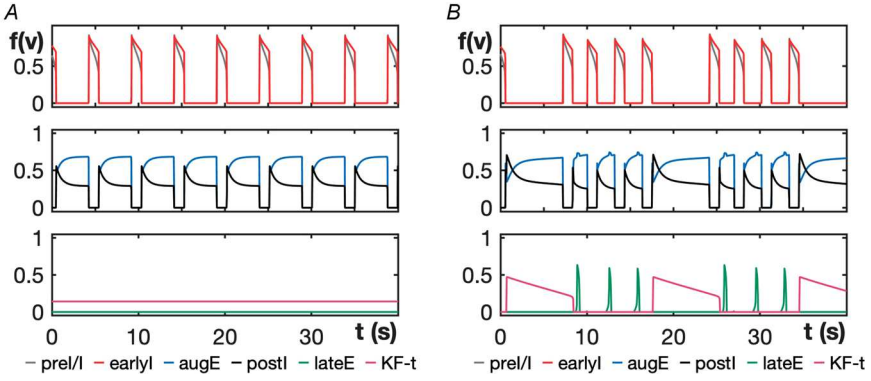

Figure 2. Tonic model output patterns
A, normal respiratory rhythm for the default parameter values given in Table 1. *B*, periodic breathing when recurrent inhibition is shut off, $\beta_6 = 0.0$ (simulated RTT). KF engages in slow oscillations (pink trace, bottom subplot) that drive prolonged E phases. [Colour figure can be viewed at wileyonlinelibrary.com]

the silent phases, or inter-burst intervals, in the oscillatory case. This difference causes the respiratory cycles that occur in between apnoeas within periodic breathing (Fig. 2*B*) to be shorter than the normal cycle periods seen in eupnoeic breathing (Fig. 2*A*), consistent with experimental observations under RTT-like conditions (Abdala et al., 2016).

We used nullcline analysis to better understand which forms of inhibition to KF-t could support the generation of the activity patterns that we expect based on experimental findings and to explain why the tonic KF-t output switches to an oscillatory pattern when inhibition is reduced in a sustained way. We see in Fig. 3 that KF-t, as modelled by Equation (2), has a cubic v_6-nullcline (continuous blue line). The m_6-nullcline (continuous red line) intersects the active branch of the v_6-nullcline for default parameter values, corresponding to a stable equilibrium point at $v_6 \approx -42$ (solid black diamond). Notice in Fig. 3*A* that when we reduce the recurrent or self-inhibition within the KF-t (lower β_6), the slow nullcline intersects the middle branch of the v_6-nullcline, destabilizing the equilibrium point and leading to oscillatory behaviour of KF-t. The oscillatory trajectory of the KF-t unit in this regime is outlined with grey lines in the figure panel. The trajectory oscillates between the left and right stable branches of the fast v_6-nullcline. The reduction of tonic inhibition (b_6) that comes in from outside to the KF-t, in contrast, does not depend on the output of the KF-t unit and hence shifts the v_6-nullcline vertically, which does not induce a transition in the stability of the equilibrium point and hence does not lead to KF-t oscillations (Fig. 3*B*). Thus, we henceforth assume for this model that the recurrent inhibition strength β_6 is non-zero in the eupnoeic regime and decreases in the RTT condition, which represents a prediction of this work, and for simplicity we assume that the tonic inhibition strength $b_6 = 0$, since this form of inhibition is not necessary to explain experimental observations.

While Figs 2 and 3 illustrate the extreme case of full removal of the inhibition to KF-t in the tonic model ($\beta_6 = 0$), Fig. 4*A* and *B* show the periodic breathing exhibited by the tonic model at the partially reduced inhibition levels $\beta_6 = 0.025$, which is near the value where KF-t transitions from tonic to oscillatory behaviour, and $\beta_6 = 0.015$. For these intermediate inhibition levels, although the KF-t equilibrium point lies on the middle branch of the v_6-nullcline and is unstable, its position is in between the two intersection points shown in Fig. 3*A*; that is, it lies closer to the local maximum of the v_6-nullcline. The proximity of the equilibrium and the m_6-nullcline to this maximum means that the trajectory evolves very slowly at the end of the KF-t active phase, resulting in a longer KF-t oscillation period and larger duty cycle for larger β_6. This effect explains the prolonged KF-t oscillations in Fig. 4*A* and *B*.

Even though the KF oscillations are longer for these transitional values of β_6 than for the simulated RTT condition ($\beta_6 = 0$), notice that the actual apnoea durations are relatively short for these values and increase slightly as β_6 decreases (Fig. 4*C*). How can longer KF-t active durations produce shorter apnoeas when apnoeas in the model result from KF-t drive to the post-I unit? The key to explaining this outcome is to focus on the level of KF-t output while it is active. Our simulations show that when KF-t output is above about 0.23, it supports prolonged post-I activity corresponding to apnoeas. When KF-t output falls below this value, closer to levels comparable to the output in the tonic regime with $\beta_6 = 0.05$, the normal respiratory rhythm takes over. For intermediate β_6 near the transition to KF-t

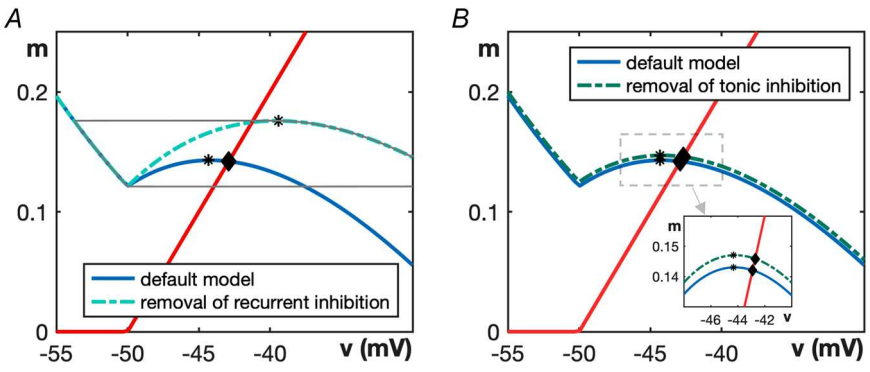

Figure 3. Tonic KF-t model in the phase plane
A, the default model has a stable equilibrium point with $v_6 \approx -42$ mV (black diamond), corresponding to tonic activity. When the recurrent inhibition to KF-t is removed, the local maximum (black asterisk) of the resulting v_6 nullcline (blue dashed curve) shifts to the right of the slow nullcline (red curve). Oscillations emerge in KF-t in this case (grey orbit). *B*, the v_6 nullcline shifts upwards when tonic inhibition is removed as shown by the dashed blue curve. KF-t remains tonic in this case since the local maximum of the v_6 nullcline (black asterisk) remains on the left of the equilibrium point (see also zoomed view in inset). [Colour figure can be viewed at wileyonlinelibrary.com]

oscillations, during each prolonged KF-t active period, KF-t output relatively quickly reaches close to the tonic level and plateaus. Thus, apnoea duration is relatively short. When β_6 is reduced from there, although KF-t active phases become shorter, the amplitude of each oscillation increases (see Fig. 3*A*) and it takes longer for KF-t output to decrement to tonic levels. Therefore, even though the KF-t burst duration decreases when inhibition is lowered, the apnoea duration increases. As a final subtlety, we note that the actual apnoea duration plotted in Fig. 4*C* (green curve) is not monotonic. This non-monotonicty arises because the apnoea duration

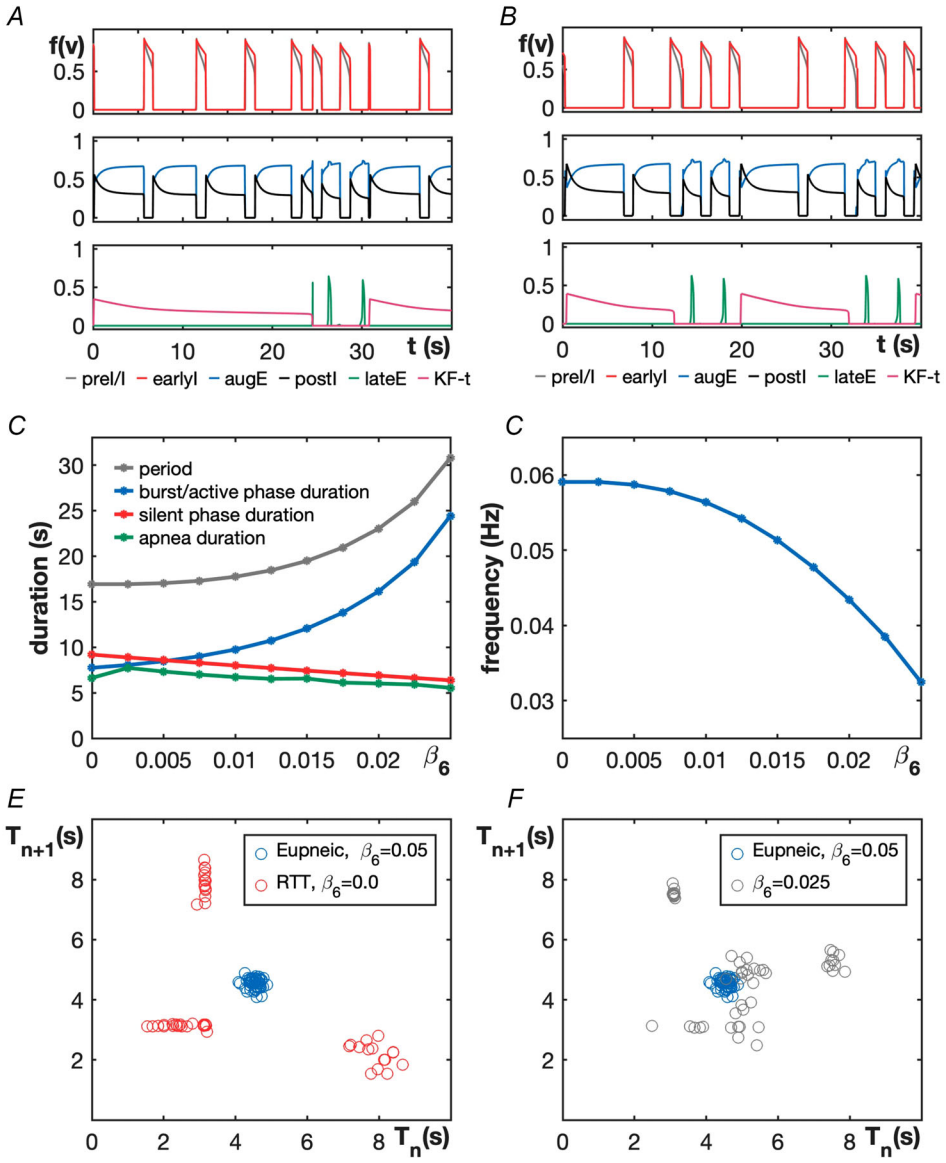

Figure 4. Tonic model output depends on the level of recurrent inhibition within the KF-t population (β_6)
A, respiratory pattern with a recurrent inhibition strength near the point of transition of KF-t from tonic to oscillatory ($\beta_6 = 0.025$). *B*, respiratory pattern with recurrent inhibition strength $\beta_6 = 0.015$, representing an intermediate case between that shown in *A* and the RTT condition shown in Fig. 2*B*. *C*, when β_6 is decreased, the period of KF-t oscillations and its burst or active phase duration decreases while apnoea duration remains roughly the same but slightly increases. *D*, apnoea frequency, defined as KF-t burst frequency (i.e. the inverse of the period of oscillations), rises as the inhibition level to KF-t decreases. *E*, total respiratory cycle duration during the $(n+1)^{st}$ cycle relative to the n^{th} cycle for the tonic model with noise, $\beta_6 = 0.05$ (default value, blue circles) and $\beta_6 = 0.0$ (RTT, red circles). *F*, total respiratory cycle duration during the $(n+1)^{st}$ cycle relative to the n^{th} cycle for the tonic model with noise, $\beta_6 = 0.05$ (default value, blue circles) and $\beta_6 = 0.025$ (grey circles). [Colour figure can be viewed at wileyonlinelibrary.com]

also depends on the phase of post-I activity when KF-t becomes active. Regardless of this phase, post-I stays active for a similar amount of time after KF-t activation occurs, based on the level of KF-t output. Thus, when KF-t activation occurs relatively late within the E phase, the overall apnoea will be long, and this phase relation need not vary monotonically with β_6.

Since KF-t output falls to near tonic levels during each KF-t active phase, we only count the first post-I active period within each of these KF-t cycles as an apnoea. Thus, the frequency of apnoeas increases as the recurrent inhibition β_6 is lowered from 0.025 (Fig. 4*D*). These findings match the experimental results reported previously (Abdala et al., 2016; Koolen, 2021).

To further study burst patterning and transitions in activity patterns when recurrent inhibition to KF-t is lowered, we modified the tonic model to include additive Gaussian noise in the voltage equation $\sigma = 1$ in Equations (1) and (2), as described in Methods. Figure 4*E* and *F* shows the total respiratory duration (i.e. from one E onset to the next) during the $n + 1^{\text{th}}$ burst relative to the duration for the n^{th} burst (T_{n+1} versus T_n) for inhibition levels $\beta_6 = 0.0$ (RTT) and $\beta_6 = 0.025$ (just after the onset of KF-t oscillations) along with the same information for the default value $\beta_6 = 0.05$. During normal breathing (blue circles), this level of noise induces little variability in the respiratory period (which takes values between 4 and 5 s). In the case of RTT (red circles), respiratory periods cluster around two values, one corresponding to long apnoeas each having a duration of nearly 8 s and the other to shorter normal breathing periods of approximately 3 s. The reason that the normal, non-apnoeic respiratory bursts in RTT are shorter than those defined for the default model parameters is that, as we pointed out with respect to Fig. 4, the inter-burst KF output level within KF-t oscillations is much lower than its tonic output level at the baseline level of inhibition.

For the sub-normal inhibition level $\beta_6 = 0.025$ (grey circles) considered in Fig. 4*F*, the durations of the longest post-I cycles are generally shorter than the prolonged apnoeas in the RTT case (Fig. 4*F*, red circles), as discussed above. In the intermediate case, as we have also discussed already, each post-I cycle duration depends on the gradually declining KF-t output level (Fig. 4*A*), and hence there is much more variability in the respiratory cycle duration, with less of a clear clustering of durations, than for the extreme β_6 values. These results are consistent with the findings in Abdala et al. (2016). In particular, Fig. 5*Cb* in (Abdala et al., 2016) shows that the effects of blocking KF $GABA_A$ receptors in wild-type rats are comparable to Fig. 4*E*.

Past literature has shown that a systemic application of various 5-HT_{1A}R agonists can reduce the frequency of spontaneous apnoeas and restore normal respiratory function to various degrees in the murine model of RTT (Abdala et al., 2010; Dhingra et al., 2016). These agonists can potentially boost a potassium current and thus enhance tonic inhibition within the KF (Levitt et al., 2013). They can also facilitate glycinergic neurotransmission (Shevtsova et al., 2011) or opening of chloride channels (Manzke et al., 2010), each of which may underlie an increase in recurrent inhibition. In Fig. 5*A*, we show nullclines for the KF-t unit, comparing the RTT scenario in which KF-t is oscillatory to a case with increased recurrent inhibition. The slow nullcline (continuous red line) intersects the middle branch of the v_6-nullcline. This comparison repeats that given in Fig. 3*A*, showing that if recurrent inhibition to KF-t (β_6) increases, the

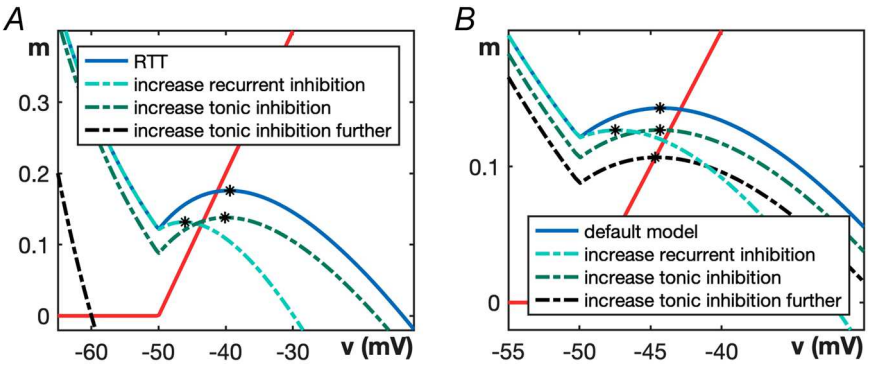

Figure 5. *A*, starting with oscillatory KF-t (RTT), $\beta_6 = 0.0$
When recurrent inhibition, β_6, is increased from 0.0, KF-t becomes tonic. When tonic inhibition, b_6, is increased, KF-t remains oscillatory. When it's increased further, it becomes silent. *B*, tonic model with inhibition increased above baseline. When recurrent inhibition is increased, KF-t remains tonic with its equilibrium point on the right branch of the v_6-nullcline but the point moves to a lower v_6 value, corresponding to less KF output. When tonic inhibition is increased, the equilibrium point moves to the middle branch and destabilizes, and thus a transition from tonic KF output to KF oscillations occurs. [Colour figure can be viewed at wileyonlinelibrary.com]

tonic KF activity is restored, which implies that periodic breathing will switch back to the normal breathing pattern. On the other hand, from the RTT condition, increasing the external tonic inhibition (b_6) to KF-t does not switch the nullcline intersection off of the middle branch (Fig. 5*A*, dashed v_6-nullcline) and hence maintains the oscillatory KF activity, until with a sufficient increase in b_6 the intersection moves to the left branch of the v_6-nullcline (Fig. 5*A*, dash-dotted v_6-nullcline) and stabilizes. This stable equilibrium point location implies that KF-t becomes fully inactive and no longer supports normal breathing.

Overall, these simulations indicate that a reduction in the recurrent inhibition to the KF neurons that provide tonic input to the ventromedullary neurons can trigger episodic apnoeas and drive breathing irregularities. In this scenario, reduction of tonic inhibition to the KF does not produce similar effects.

Emergence of active expiration. Expiration is a process that becomes active in conditions of increased respiratory drive. Exposure to low oxygen (hypoxia) or high carbon dioxide levels (hypercapnia) triggers active expiration with the recruitment of abdominal muscles during the late part of the E2 phase (i.e., late expiration, or late-E) to improve pulmonary ventilation (Molkov et al., 2014). Decreased KF activity is known to play a role in the emergence of late-E abdominal activity (Barnett et al., 2018; Jenkin et al., 2017). Moreover, Koolen (2021) showed that systemic administration of the 5-HT_{1A}R agonist NLX-101 increases the respiratory drive, elevating the respiratory frequency and causing the appearance of active expiration (late-E activity) under resting conditions.

We first consider the phenomenon of late-E activation. The tonic model has an excitatory synaptic connection from KF-t to post-I and an inhibitory connection from post-I to late-E (see Fig. 1*A*). This architecture suggests that when there is a reduction in KF activity, a decrease in post-I output will result, which in turn will reduce the post-I dependent inhibition to late-E. If KF-t output is reduced sufficiently, then late-E should start spiking. This logic leads us to consider the input-related mechanisms by which 5-HT_{1A} agonists may strengthen inhibition in the KF. In Fig. 5*B*, we analyse the effect of increasing each of the two different types of inhibition to KF-t. Initially, the KF-t unit has a stable equilibrium at $v_6 \approx -42$. When we increase recurrent inhibition, the slow nullcline (shown in red) still intersects the modified v_6-nullcline (shown in dashed blue) on its right branch, leading to a stable tonic equilibrium (Fig. 5*B*). In this case, however, the stable equilibrium has a lower v_6 value than originally. Therefore, we see that increasing recurrent inhibition, β_6, reduces the tonic output level $f_6(v_6)$ of KF-t and eventually causes KF-t output to turn off. If we instead turn on and increase tonic inhibition to KF-t ($b_6 > 0$), notice in Fig. 5*B* that at first a small reduction in the v_6-coordinate of the equilibrium point and hence in $f_6(v_6)$ occurs, but this is not sufficient to promote late-E activity. With an additional increase in b_6, the equilibrium point moves to the middle branch of the v_6-nullcline and KF-t becomes oscillatory, leading to continued late-E suppression. Therefore, to see the emergence of late-E spiking in the tonic model, we gradually increased the recurrent inhibition (β_6) to KF-t and kept $b_6 = 0$.

For the parameter values given in Table 1, there is no late-E activation, as seen in Fig. 2*A*. An emergence and quantal acceleration of late-E activity with increasing β_6 are illustrated in Fig. 6. When we increase β_6 to 0.3 (Fig. 6*A*), late-E spikes once during every three post-I bursts. For $\beta_6 =$ 0.6 (Fig. 6*B*), late-E spikes once during every two post-I bursts. Increasing β_6 to 1.8 (Fig. 6*C*) results in a late-E spike during every post-I burst. The increasing late-E spiking frequency with respect to β_6 is summarized in Fig. 6*D*. This figure plots the ratio of the number of late-E spikes to the number of post-I bursts on the y-axis. For example, at $\beta_6 = 1.2$, the ratio is 2/3, corresponding to two late-E spikes during every three post-I bursts.

In the experiments of Koolen (2021), this increase was largely due to a decrease in the post-I duration while the duration of pre-I oscillations remained roughly the same. Under increases in β_6, our tonic model reproduces these findings; indeed, we can see in Fig. 6 that the E phase becomes shorter as β_6 increases from panel *A* to panel *C* (see middle subplots), due to the reduced KF excitation to post-I, while the I phase duration essentially does not change (see top subplots). These results are quantified across a range of β_6 values in Fig. 7. Overall, the fact that our model results parallel the data from previous experiments indicates that the assumptions we have made in constructing the tonic model, including the importance of recurrent inhibition within the KF-t populations, are plausible and suggests that our findings may be useful to guide future experiments.

Silent model

In contrast to the tonic model, the silent model has two KF units: KF-t and KF-s. The values for all of the parameters that appear in both the tonic model and the silent model remain the same as in the tonic model (Table 1), while the values of parameters specific to the silent model are given in Table 2. With these values, KF-t is tonic, with a stable critical point for which $f_6(v_6) \approx 0.15$, and KF-s is silent, with a stable critical point below $v_{\min}$ such that its output is zero. Note that the lack of output of the KF-s unit does not reflect an inability to activate; rather, this unit remains quiescent in the baseline model

tuning relevant for eupnoeic rhythm generation, just as the late-E population does. The bursting pattern of the silent model for the default parameter values naturally matches that of the tonic model (Fig. 2*A*) since KF-s is silent. Hence, our analysis of the role of KF in active expiration resulting from increases in inhibition within the KF, and the corresponding Figs 5*B*, 6 and 7, apply for the silent model as well.

As with the tonic model, we consider nullclines for the silent model as a means to determine what forms of inhibition of the KF allow the model to match experimental findings on RTT-like respiratory patterns. Importantly, in the silent model, we assume that if the KF-s population becomes active, then it will provide drive to post-I, and in our analysis, we manipulate the inhibition to KF-s. This approach makes the silent model a distinct alternative to the tonic model. If we instead varied inhibition to the KF-t unit in the context of the silent model, then the KF-s unit would simply remain silent and hence would be irrelevant, so our results would trivially match the previous subsection.

Nullcline analysis shows that for the silent model, KF-s transitions to oscillatory behaviour when we reduce the tonic inhibition strength to the KF-s unit, b_7 (Fig. 8*A*), because this loss of inhibition causes the model to no longer have a stable fixed point in the silent phase. The same does not happen with recurrent inhibition, since KF-s is initially silent and hence receives no recurrent inhibitory input regardless of β_7; for simplicity, we fix $\beta_7 = 0$ in our default parameter set. In the subsequent subsections, we will consider the effects of reduced tonic inhibition in the silent model.

Before considering effects of reduced inhibition in the silent model, we note that once tonic inhibition is reduced, increasing it restores the normal breathing rhythm (Fig. 8*B*). On the other hand, starting from the case of reduced tonic inhibition and introducing a small amount of recurrent inhibition keeps KF-s in an oscillatory state, and a further increase in b_7 causes the v_7-nullcline to become monotonic. Once this occurs, the KF-s system has a stable critical point at a v_7 level such that $f_7(v_7) > 0$, corresponding to a tonic KF-s output (Fig. 8*B*). Overall, in contrast to the tonic model, which suggests that inhibition within the KF is recurrent and hence depends on KF activity levels, the silent model suggests that inhibition to KF respiratory neurons is sustained and arrives from an outside source. Future experimental determination of the nature of inhibition to KF respiratory neurons will help to distinguish which, if any, of our models is consistent with the biological reality.

When the tonic inhibition, b_7, to KF-s is reduced in the silent model, KF-s activity transitions from quiescent, with a stable critical point on the left branch of the v_7-nullcline, to oscillatory, with an unstable critical point on the middle branch (Fig. 8*A*). The oscillations in KF-s provide oscillatory drive to post-I and produce a periodic

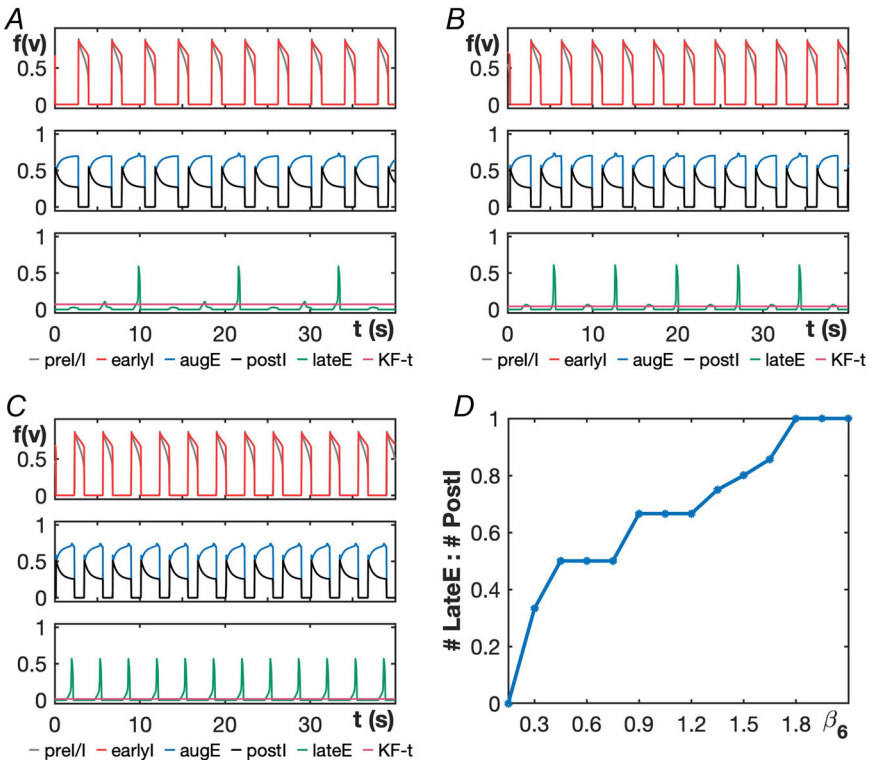

Figure 6. Quantal acceleration of late-E in the tonic model
A–C, burst patterns exhibited by the tonic model at different inhibition levels. *A*, $\beta_6 =$ 0.3. *B*, $\beta_6 = 0.6$. *C*, $\beta_6 = 1.8$. *D*, the late-E spiking frequency increases with respect to the recurrent inhibition strength β_6. [Colour figure can be viewed at wileyonlinelibrary.com]

breathing pattern similar to that observed in RTT. At the minimal value of $b_7 = 0$, which we will refer to as our silent model representation of RTT, the apnoeic breathing pattern exhibited by the model is shown in Fig. 9*A*. In contrast to the output of the KF-t model (Fig. 2*B*), the KF-s model does not produce late-E activation during RTT. The onset of periodic breathing, as b_7 is reduced in the silent model, occurs at $b_7 \approx 0.015$ and the burst pattern just below this inhibition level is shown in Fig. 9*B*. In Fig. 9*C* and *D* we plot the period of KF oscillations, the apnoea duration and the apnoea frequency as the inhibition strength b_7 is varied. The apnoea duration remains roughly constant and is non-monotonic in b_7 (shown in green in Fig. 9*C*), whereas the apnoea frequency increases as b_7 decreases (Fig. 9*D*). These results agree qualitatively with the results for the tonic model (Fig. 4*C* and *D*).

Recall from Figs 2*B* and 4*A*, *B* that as the inhibition level decreases in the tonic model, the KF-t burst/active phase duration decreases while the silent phase duration remains roughly the same. This causes the period of KF-t oscillations to decrease and apnoea frequency to increase. In the silent model, however, we see in Fig. 9*A* and *B* that the period of KF-s oscillations decreases mainly due to the reduction of silent phase duration of KF-s when b_7 is lowered from 0.015. This effect arises because with less inhibition, the v_7-nullcline in the silent phase moves farther away from the m_7-nullcline (Fig. 8*A*), which yields less of a delay in the jump-up to the active phase. Therefore, this is another distinction between the tonic and silent models.

To study burst patterning in the silent model, we modified the model by adding Gaussian noise with mean 0 and standard deviation 1 by setting $\sigma = 1$ in Equations (1) and (2). Figure 9*E* shows the total respiratory duration during the $(n+1)^{st}$ burst relative to the duration for the n^{th} burst (T_{n+1} versus T_n) for inhibition levels $b_7 = 0.0$ (RTT), $b_7 = 0.014$ (just after the onset of KF-s oscillations), and $b_7 = 0.02$, the default value. The model did not show much variability in respiratory periods (blue circles in Fig. 9*E*) during normal breathing conditions, as expected. Notice in Fig. 9*A* that during KF-s oscillations, the inter-burst KF-s output matches the KF-s output level (≈ 0) during normal breathing. Therefore, in the RTT regime in this model, we expect that the breathing cycle durations in between apnoeas will remain the same as in the eupnoeic case. Aligning with this expectation, in the RTT case, we observe two different respiratory cycle durations (red circles in Fig. 9*E*): apnoeas with duration $\approx$ 0.9 s and normal breathing cycles during the silent phase of each KF-s oscillation, which match the cycle duration with the default model. This perseverance of the normal cycle duration even in the RTT condition differs from the activity in the tonic model since in the tonic model under RTT conditions, the cycle duration in between apnoeas is shorter than the default respiratory breathing period.

For an intermediate value of inhibition in the silent model, for example $b_7 = 0.014$, the apnoeas are shorter compared with the RTT case (Fig. 9*E*). We see in Fig. 9*C*, however, that apnoea duration is clearly non-monotonic in b_7. Notice from Fig. 9*A* and *B* that for different levels of b_7, the initial KF-s activation can occur at different phases within the ongoing post-I active phase. For certain intervals of b_7, this phase shift changes smoothly, but as b_7 is decreased through other values, KF-s activation can switch from occurring early in every n^{th} post-I cycle to late in every $(n+1)^{st}$ cycle, yielding increased apnoea durations. To avoid this arbitrary phase relation, we next introduced a putative excitatory connection from the post-I unit to the KF-s unit and examined its effects.

Including this excitatory drive does not change the eupnoeic breathing pattern exhibited by the silent model, since KF-s is silent in this regime. The effects of varying inhibition on the v_7-nullcline and its intersection with the m_7-nullcline also remain unchanged, and thus we focus on effects of varying tonic inhibition to KF-s. As was the case without the drive from post-I to the KF-s unit, when the inhibition strength parameter b_7 is reduced sufficiently, the KF-s unit produces endogenous oscillations, which in turn leads to a perturbation in the normal breathing rhythm (Fig. 10*A*). The transition of KF-s from the silent to the oscillatory state now occurs at $b_7 \approx 0.02$ and the bursting pattern exhibited at this inhibitory level is shown in Fig. 10*B*. Notice that in this case, post-I activation on certain cycles immediately recruits KF-s activation, without any phase lag. This effect smooths out the dependence of apnoea duration on b_7 and results in a monotonic relationship.

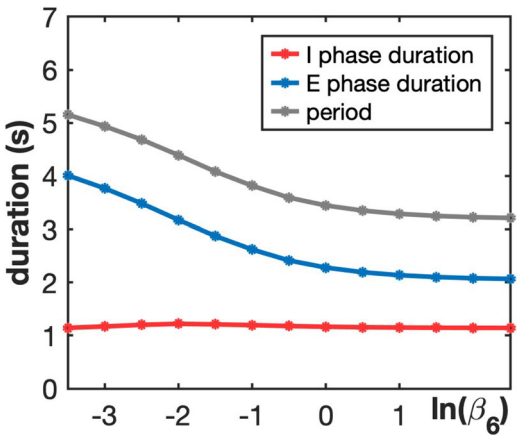

Figure 7. Durations of inspiration and expiration and overall respiratory period vary with ln (β_6) in the tonic model
The gradual decrease in the period with increasing β_6 comes from a drop in the E phase duration, whereas the I phase duration remains roughly constant. [Colour figure can be viewed at wileyonlinelibrary.com]

The results related to apnoea duration and frequency (Fig. 10*C* and *D*) qualitatively agree with those for the tonic model (Fig. 4*C* and *D*) as well as for the silent model without feedback from post-I to KF-s (Fig. 9*C* and *D*). The excitatory connection from post-I to KF causes the apnoea duration to increase steadily as b_7 is decreased in this augmented model (Fig. 10*C*) and also results in a step-like decline in KF-s period as b_7 decreases. This pattern represents a quantal effect: an approximately constant plateau occurs when KF-s activates once every n post-I cycles for fixed n, and then a step down to a lower period occurs when b_7 becomes low enough that KF-s can activate once every $n-1$ post-I cycles.

Figure 10*E* shows the burst patterning of the augmented silent model with Gaussian noise. This figure is comparable with Fig. 9*E* in that the cycle durations between apnoeas carry over from the normal case to the cases with reduced inhibition levels. The new feature here is that the additional synaptic connection makes the cycle durations less variable than they were previously.

Finally, we do not separately consider the emergence of active expiration in the silent model. Since the KF-s population is silent by default, increasing the inhibition to KF-s from its baseline state would have no effect, while increasing the inhibition to KF-t with KF-s remaining silent would simply repeat the results that we obtained with the tonic model as described in 'Emergence of active expiration'.

Discussion

In this work, we consider a family of respiratory circuit models that include the KF, designed to be minimal in terms of the complexity of the neural units, endogenous neuronal dynamics and synaptic connections involved. We show that two of these models capture the central experimental findings on the response of respiratory patterns to manipulations involving the KF: (1) reduction of GABA-mediated inhibition to KF neurons induces periodic or intermittent breathing with apnoeas (Abdala et al., 2016; Dhingra et al., 2016), with an apnoea frequency and other properties that vary with the strength of inhibition within the KF; (2) durations of apnoea events are maintained or lengthened with reductions in the inhibition level to KF (Abdala et al., 2016; Dhingra et al., 2016); (3) when intermittent breathing occurs, increases in KF inhibition can induce eupnoea (Abdala et al., 2010, 2016); (4) from the eupnoeic state, additional increases in KF inhibition cause quantal activation of abdominal late-E activity (Koolen, 2021). Within this computational framework, we identify the synaptic connections that are compatible with the experimental results and obtain predictions about KF properties, circuit organization and respiratory neuron behaviours under various conditions that could be tested to distinguish the two models and to check their validity. Our work builds on a series of assumptions and logical inferences, supported by the literature, which we now discuss before turning to the predictions that we derive as well as model limitations and future directions.

KF as a source of breathing irregularities

Intermittent breathing, such as observed in RTT, manifests as breathing that is periodically disrupted by apnoeic episodes. These apnoeas are accompanied by abnormally strong constrictor activity to the

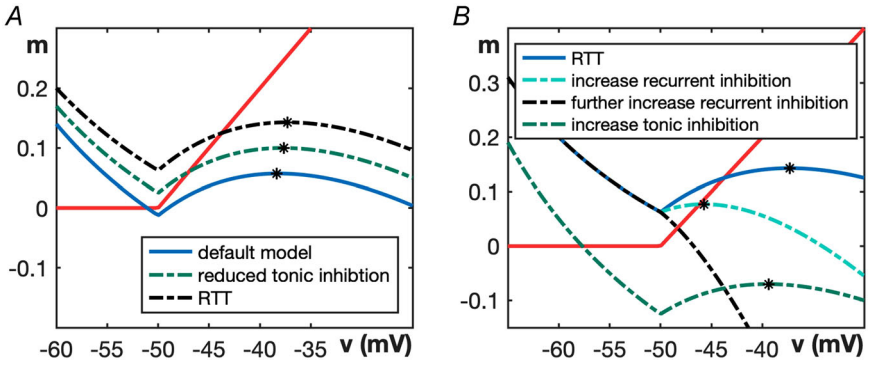

Figure 8. Phase plane analysis of impacts of altered inhibition in the silent model
A, when the tonic inhibition to KF-s is removed, the slow nullcline (red curve) intersects the middle branch of the resulting v_7-nullcline (green dashed curve). Therefore, oscillations emerge in KF-s in this case. *B*, starting with oscillatory KF-s (RTT scenario), when tonic inhibition is increased, KF-s becomes silent (i.e. nullclines intersect on left branch of dashed green v_7-nullcline). When recurrent inhibition is increased, KF-s remains oscillatory (intersection on middle branch of cyan dashed v_7-nullcline). When it is increased further, KF-s becomes tonic (montonic black v_7-nullcline). [Colour figure can be viewed at wileyonlinelibrary.com]

upper airways driven by motor neurons that exhibit a post-inspiratory activity pattern during regular breathing (Abdala et al., 2010; Stettner et al., 2007; Voituron et al., 2010). Post-inspiratory activity strongly depends on excitatory outputs from the KF (Dutschmann & Herbert, 2006; Smith et al., 2007). Disruption of inhibitory transmission in the KF, causing disinhibition, leads to periodic breathing with periods of excessive post-inspiratory activity to the larynx (Abdala et al., 2016; Dhingra et al., 2016). These findings provide strong (yet indirect) evidence that intermittent breathing can result from periodic KF overactivation on a time scale slower by an order of magnitude than respiration. Such a slow timescale suggests that the emerging oscillations can originate within the KF, resulting from a combination of intrinsic neuronal properties and synaptic inputs to the

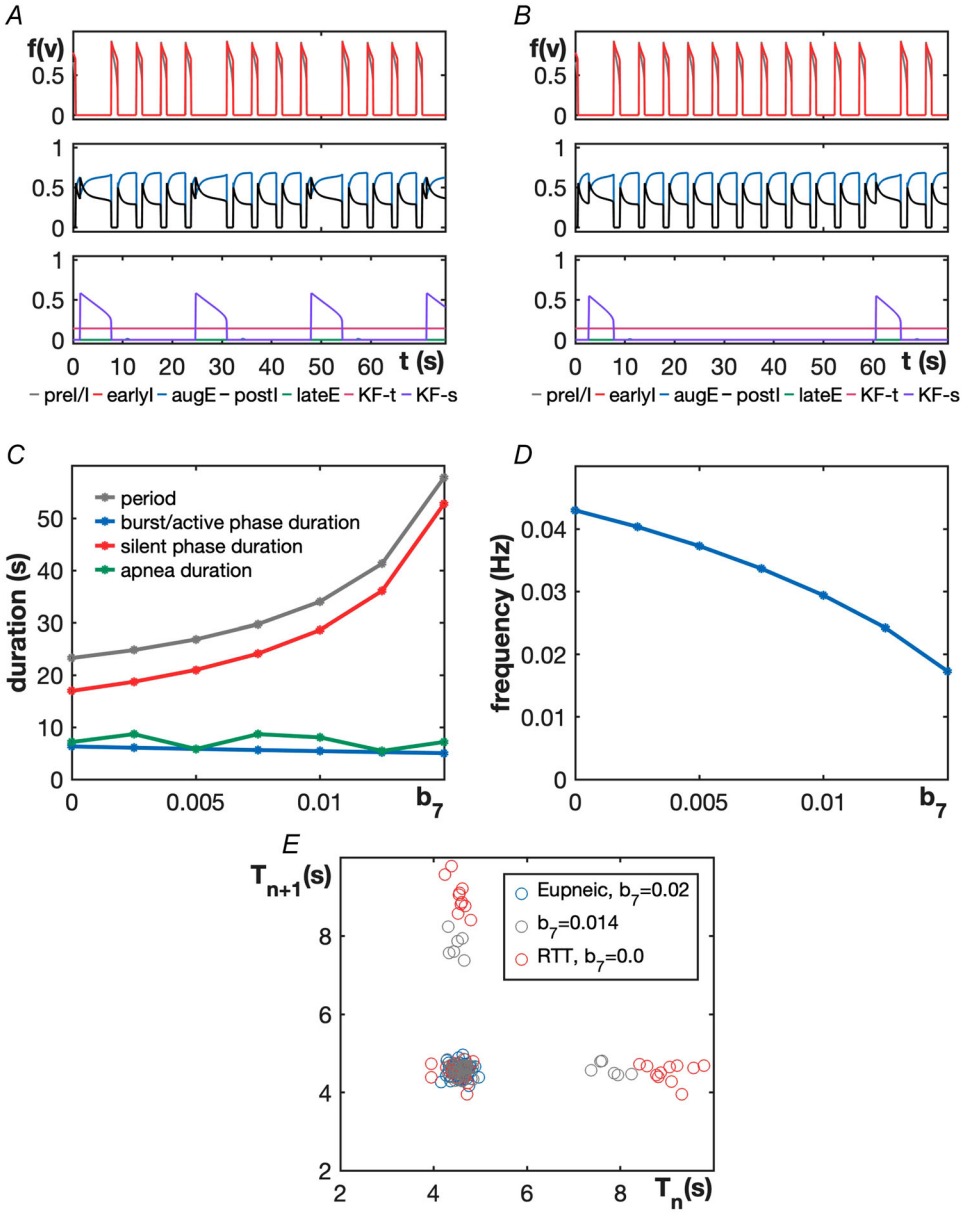

Figure 9. The silent model exhibits apnoeas, with preservation of normal cycle durations in between them, as tonic inhibition is reduced
A, periodic breathing exhibited by the model for $b_7 = 0.0$ (RTT). *B*, respiratory pattern at an inhibition value near the point of transition of KF-s from tonic to oscillatory ($b_7 = 0.014$). *C*, the period of KF-s oscillations, KF-s burst/active phase duration, silent phase duration and apnoea duration with respect to b_7. *D*, apnoea frequency, which is equal to the inverse of the period of KF-s oscillations, increases as the inhibition level to KF-s decreases. *E*, total respiratory duration during the $(n + 1)^{st}$ burst relative to that in the n^{th} burst for silent model 1 with noise with $b_7 = 0.02$ (default value), $b_7 = 0.014$, and $b_7 = 0.0$ (RTT). [Colour figure can be viewed at wileyonlinelibrary.com]

region. Our work illustrates some possible mechanisms that could give rise to this patterned KF activity.

Baseline activity in the KF

KF contains a large population of glutamatergic neurons that connect with the rCPG (Geerling et al., 2017). A recurrent excitatory network endowed with spike frequency adaptation properties (i.e. exhibiting a reduction in firing frequency within ongoing spiking activity) has the capacity to produce population-based rhythmic bursting. Changing parameters can transition such a system to a bursting regime regardless of whether it initially lies in a silent or tonically active state with a steady activity level. Therefore, we consider two basic KF network configurations. In the first configuration

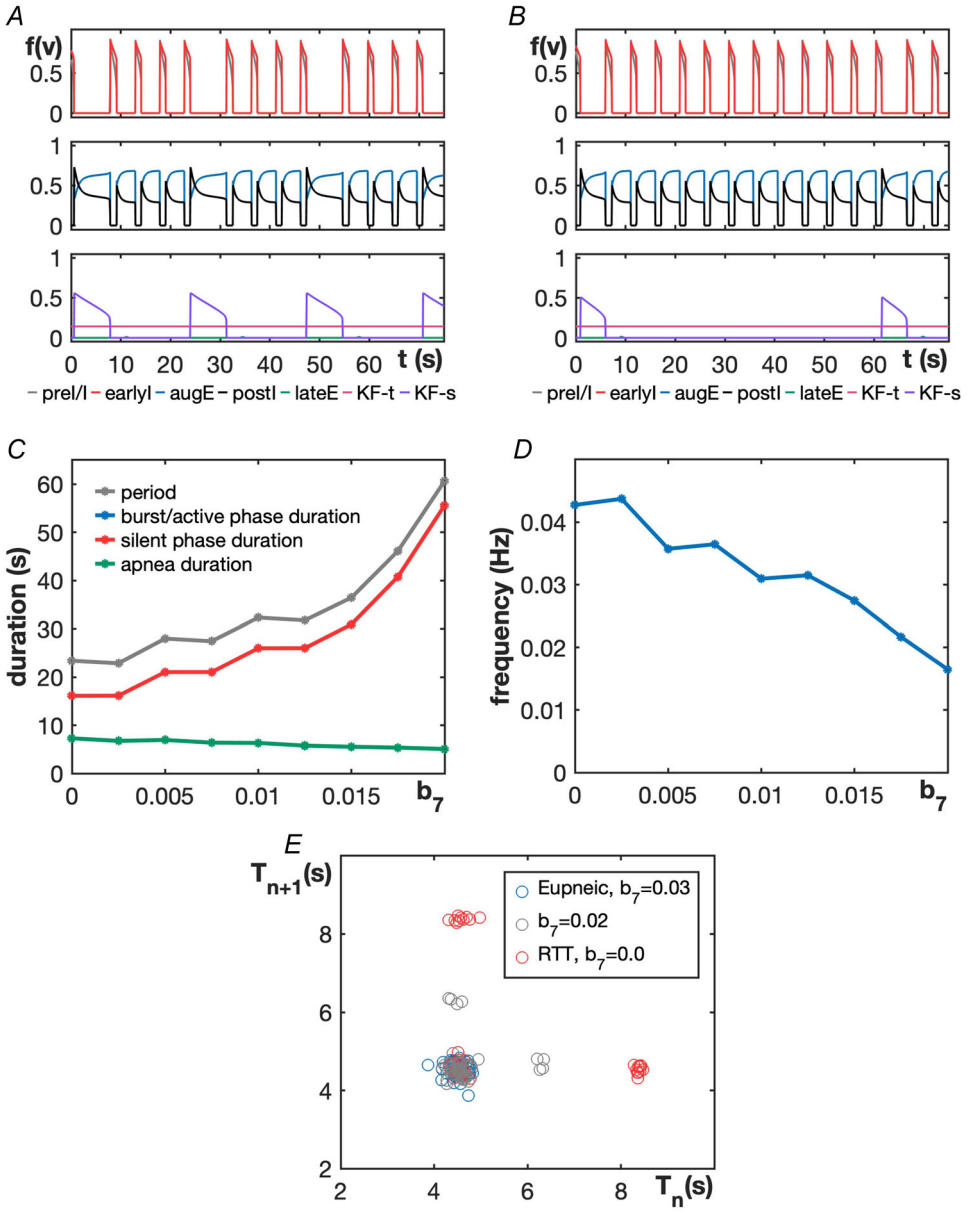

Figure 10. The inclusion of excitatory drive from post-I to KF-s reduces the variability in cycle durations
A, periodic breathing exhibited by the model for $b_7 = 0.0$ (RTT). *B*, respiratory pattern at an inhibition value near the point of transition of KF-s from tonic to oscillatory ($b_7 = 0.02$). *C*, The period of KF-s oscillations, KF-s burst/active phase duration, KF-s silent phase duration and apnoea duration with respect to b_7. In this case, the blue curve is identical to and completely hidden by the green curve, due to the connection from post-I to KF-s. *D*, apnoea frequency increases non-monotonically as the inhibition level to KF-s decreases. *E*, total respiratory duration during the $(n + 1)^{st}$ burst relative to that in the n^{th} burst when noise is included, with $b_7 = 0.03$ (default value), $b_7 = 0.02$ and $b_7 = 0.0$ (RTT). [Colour figure can be viewed at wileyonlinelibrary.com]

(*tonic model*), KF is represented by a single population with a tonic activity pattern under baseline conditions, which can transition into a bursting regime by relevant perturbations. In the second configuration (*silent model*), KF includes a subpopulation that is quiescent at baseline, either due to a balance of endogenous currents that is inadequate to induce spiking without boosts in excitatory drive or due to suppression by ongoing inhibition but starts producing oscillatory activity as parameters change. In the latter case, we assume that there is another population of neurons in the KF that always produces tonic output to provide the necessary excitatory drive to the rCPG. Still, unlike in the tonic model, this population does not become oscillatory under the manipulations that we consider.

Sources of GABA-mediated inhibition

Experiments show that reduced GABAergic inhibition in the KF leads to the emergence of slow oscillations modulating rCPG activity and causes breathing irregularities (Abdala et al., 2016). Depending on the KF network configuration, we infer different origins of this inhibition. Specifically, in the tonic model, this inhibition appears to be recurrent. Although we implement this recurrence as self-inhibition in our minimal model, this recurrent inhibition is a reduced representation of a scenario in which the KF population excites inhibitory interneurons that in return provide feedback inhibition. The location of these inhibitory interneurons is not specified by our model. One can speculate that these neurons can represent a local inhibitory subpopulation providing negative feedback within the KF for self-regulation. Alternatively, they could be located in another site, such as the BötC or the parabrachial nucleus, proved to have recurrent connectivity with KF (Ezure et al., 2003; Gaytan et al., 1997; Varga et al., 2021). In contrast, in the framework of the silent model, the GABAergic inhibition in KF is predicted to take the form of a tonic or sustained drive, probably originating externally to the KF; for example, the NTS is known to send feedforward inhibitory projections to the KF and hence could represent the source of this input (Kubin et al., 2006; Otake et al., 1992).

Mechanisms of 5-HT$_{1A}$ inhibition

Experimental evidence indicates that manipulating 5-HT$_{1A}$ receptors in the KF produces changes in respiratory activity comparable to the changes induced by modulating GABAergic inhibition (Abdala et al., 2016; Dhingra et al., 2016). Specifically, 5-HT$_{1A}$ antagonists evoke intermittent breathing while 5-HT$_{1A}$ agonists can reduce breathing irregularities or even restore eupnoea (Besnard et al., 2012; Dhingra et al., 2016). While serotonergic inputs originate outside of the KF (e.g. in the raphe nucleus), their functional effects, mediated by 5-HT$_{1A}$ receptors, are compatible with both the recurrent and tonic inhibition scenarios. Specifically, tonic inhibition could be by membrane hyperpolarization due to the activation of 5-HT$_{1A}$R-coupled potassium channels (Montalbano et al., 2015), which is compatible with the silent model. On the other hand, another known impact of 5-HT$_{1A}$R activation is the enhancement of glycinergic inhibition in neurons that express the GlyR α3 subunit (Manzke et al., 2010; Shevtsova et al., 2011). This mechanism could be involved in altering the recurrent inhibition provided by glycinergic interneurons. Potentially, the interneuron population could coexpress both GABA and glycine and thus could mediate the effects of both GABAergic and serotonin-modulated recurrent inhibition in the tonic model. Finally, our results on the emergence of active expiration (see 'Emergence of active expiration') suggest that 5-HT$_{1A}$ agonists may strengthen the recurrent inhibition within a tonic population of KF neurons.

Additional predictions and implications

Both the tonic and silent models, with appropriate forms of inhibitory connections, capture the set of benchmarks that we initially imposed. While it is not feasible to use these models for quantitative predictions, our modelling framework can allow us to propose experimental designs that can be deployed to test and select between these models. For starters, the structural differences that distinguish the two models themselves represent predictions. Specifically, the tonic model assumes that the KF would feature prominent recurrent inhibition, through which increased activity in KF neurons strengthens the inhibitory inputs that these neurons receive. In contrast, the silent model predicts an important role for a sustained inhibitory input to KF from an outside source, as well as the presence of a subpopulation of KF neurons that exhibit little or no activity under control states of eupnoeic respiration.

The network configurations predicted by the two models also have different implications for abdominal activity during periods of intermittent breathing when inhibition in KF is compromised. Indeed, in the tonic model, reduction in recurrent inhibition transforms steady KF activity into an oscillatory regime with periods of overactivity inducing temporary apnoea, adaptation to near a normal activity level, and then periods of silence (see Fig. 4*A* and *B*). During the latter periods, KF does not provide excitation to post-inspiratory neurons in BötC, which results in a disinhibition of expiratory neurons in pFL and evokes abdominal late-E activity that drives

active expiration (Fig. 4*A* and *B*). In contrast, in the silent model, oscillations in KF emerge in a previously silent population while the steady activity of the tonic KF subpopulation remains unaltered. Therefore, conditions for the abdominal activity breakthrough are never created (see Fig. 9*A* and *B*). Interestingly, some apnoeic events in some RTT mice are accompanied by abdominal activation without a clearly corresponding late-E activation (Abdala et al., 2010), but this result does not suffice to distinguish the two models, as late-E activity could be present yet phase-shifted by other factors.

Another interesting prediction of this work is concerned with the active expiratory response to inhibition of KF in conditions of hypercapnia. High levels of CO_2 recruit abdominal muscles during expiration via activation of pFL late-E neurons through either excitation or disinhibition (Flor et al., 2020; Pagliardini et al., 2011; Zoccal et al., 2018). According to the model, under hypercapnic conditions KF inhibition leads to lesser activation of post-I neurons in the BötC, which, in turn, disinhibits the pFL late-E population. The late-E neurons also receive additional CO_2-dependent excitatory chemosensory drive (Molkov et al., 2010; Rubin et al., 2011), which would be synergistic with late-E disinhibition. Therefore, in the model, the dependence of the late-E frequency on KF inhibition shown in Fig. 6*D* would progressively shift to the left with a gradual increase in the chemosensory drive. Experimentally, the central chemosensory drive corresponds to the CO_2 concentration, and different levels of KF inhibition were achieved by Koolen (2021) by varying doses of a $5HT_{1A}R$ agonist. So, we predict that in mild hypercapnia, the quantal acceleration of late-E activity in the Koolen (2021) experiments would occur at lower concentrations of $5HT_{1A}R$ agonist.

Typically, experiments relating to respiration in RTT and under compromised KF inhibition compare across two groups, such as control *versus* experimental mice or wild-type *versus* knock-out mice. Using computational models allows us to generate predictions about the effects that we expect from gradual changes that induce states in-between the extreme endpoints. In the tonic model, reductions in inhibition to KF induce a regime of KF oscillations with a long epoch of sustained KF activity within each cycle. In this regime, apnoeas are interspersed with respiratory cycles with a mix of durations, including some slightly longer and some slightly shorter than those seen under control conditions (Fig. 4). Further decreases in inhibition are predicted to shorten the KF active duration and the oscillation period, with a small increase in apnoea duration and a regularization of cycle durations in between apnoeas. The silent model points to a different pattern of changes with progressive decrease in inhibition to KF. In this model, we see that when the onset of apnoeas occurs, the durations of the cycles in between the apnoeas are fairly stereotyped and match those seen in control conditions (Fig. 9). Decreasing inhibition allows apnoea durations to show a net increase, but unlike in the tonic model, this relationship is non-monotonic. If we hypothesize the inclusion of an additional excitatory connection from BötC neurons to the quiescent KF population, then we recover a more consistent phase relation between expiratory BötC and KF activity, which regularizes the trend in apnoea durations (Fig. 10).

In summary, the tonic and silent models are both consistent with published experiments but can be differentiated in terms of their predictions about KF activity in baseline conditions, inhibitory pathways that impact KF activity, and alterations in respiratory patterns resulting from decreases as well as increases in inhibition to the KF. Finally, an interesting possibility that should also be kept in mind is that the tonic and silent models may both be valid but in different regimes of respiratory circuit function; for example, changes under vagotomy may alter KF activity in a way that corresponds to switching between these two models. These possibilities require experimental verification to be validated.

Model limitations and future directions

By starting from a minimal modelling framework, we were able to use analytical tools, including analysis of nullclines in certain phase planes, to argue against the presence of specific combinations of KF endogenous dynamics and forms of inhibition to the KF, while also providing a proof of principle that certain other configurations can capture a range of experimental findings and merit further consideration. A natural next computational step would be to address the limitations of this minimal modelling framework by implementing the proposed circuit arrangements in a more complete model featuring populations of spiking neurons with a full complement of known transmembrane ion currents in each of the constituent brain regions as well as more biologically detailed synaptic interactions. Past work has shown that endowing KF neurons with intrinsic bursting capabilities and also assuming the presence of certain synaptic interactions between neurons in the KF, in the parabrachial nucleus (PBN), and in the BötC produces a circuit that also produces eupnoeic respiratory output and captures the effects of vagotomy as well as periodic breathing following reduction of GABAergic inputs to the KF (Wittman et al., 2019). Because these ideas were considered previously and represent a specific set of assumptions that go beyond our minimal framework (e.g. involvement of a PBN component), we did not consider these properties in this work. While the results that we obtained show that endogeneous KF oscillations are not necessary to explain experimental findings, since previous studies have demonstrated the presence of KF neutrons with

Table 3. Qualitative differences of the 'tonic' and 'silent' models

'Tonic' model	'Silent' model
KF contains an excitatory, recurrently interconnected population with tonic baseline activity	KF is represented by two subpopulations, one of which is tonic and the other of which is silent at baseline
KF neurons receive recurrent GABAergic inhibition (phasic with their own activity). Reduction in this inhibition leads to bursting	Both populations receive tonic GABAergic inhibition (independent of their own activity); reduced inhibition makes the silent population oscillate
KF neurons express $5HT_{1A}R$, the activation of which facilitates recurrent inhibition in the KF population (e.g., glycinergic)	$5HT_{1A}R$ activation tonically inhibits KF activity (e.g. through direct membrane hyperpolarization)
Predicts breakthrough of late-E activity during RTT-like apnoeas.	No breakthrough of late-E predicted
As inhibition to KF decreases, KF active phase duration decreases	As inhibition to KF decreases, the silent phase duration of the KF-s population decreases
In RTT-like activity, cycles that lack apnoeas are shorter than the default respiratory period	In the RTT regime, cycles that lack apnoeas exhibit the same period as eupnoeic cycles

phasic discharge patterns both with and without vagotomy (Morschel & Dutschmann, 2009; Takagi & Nakayama, 1958), another natural future direction will be to compare these frameworks directly and to explore possible ways to integrate these models. Future work could also extend the model to include additional factors, such as slower forms of modulation of the respiratory circuitry, mechano-afferent drive and astrocytic effects (Occhipinti et al., 2007, 2010, 2011). Of course, future experimental work to directly derive more information about the intrinsic properties of KF neurons, their endogenous dynamics, and the synaptic interactions in which they are involved would be an invaluable complement to computational approaches. Hopefully the findings from this work and other computational studies can guide these experimental investigations in productive directions.

Conclusions

Our modelling results, tuned to capture experimental observations, highlight the importance of the KF neurons in maintaining eupnoeic breathing and support the hypothesis that disruptions in KF activity can contribute to the emergence of pathological respiratory phenotypes. Our predictions suggest two different possible circuit organizations that may be present within the KF, with neuronal subpopulations displaying distinct intrinsic characteristics and synaptic connections (see Table 3 for side-by-side comparison). These new possibilities can foster future experimental and pre-clinical studies examining in detail the proposed features and their involvement in pathological states associated with breathing irregularities, such as RTT.

References

Abdala, A. P., Dutschmann, M., Bissonnette, J. M., & Paton, J. F. (2010). Correction of respiratory disorders in a mouse model of Rett syndrome. *Proceedings of the National Academy of Sciences, USA*, **107**(42), 18208–18213.

Abdala, A. P., Toward, M. A., Dutschmann, M., Bissonnette, J. M., & Paton, J. F. (2016). Deficiency of GABAergic synaptic inhibition in the Kolliker-Fuse area underlies respiratory dysrhythmia in a mouse model of Rett syndrome. *The Journal of physiology*, **594**(1), 223–237.

Bachmutsky, I., Wei, X. P., Kish, E., & Yackle, K. (2020). Opioids depress breathing through two small brainstem sites. *eLife*, **9**, e52694.

Barnett, W. H., Jenkin, S. E. M., Milsom, W. K., Paton, J. F. R., Abdala, A. P., Molkov, Y. I., & Zoccal, D. B. (2018). The Kolliker-Fuse nucleus orchestrates the timing of expiratory abdominal nerve bursting. *Journal of Neurophysiology*, **119**(2), 401–412.

Bautista, T. G., & Dutschmann, M. (2014a). Inhibition of the pontine Kolliker-Fuse nucleus abolishes eupneic inspiratory hypoglossal motor discharge in rat. *Neuroscience*, **267**, 22–29.

Bautista, T. G., & Dutschmann, M. (2014b). Ponto-medullary nuclei involved in the generation of sequential pharyngeal swallowing and concomitant protective laryngeal adduction in situ. *The Journal of Physiology*, **592**(12), 2605–2623.

Besnard, S., Khemiri, H., Masse, F., Denise, P., Verdaguer, M., & Gestreau, C. (2012). Differential respiratory control of the upper airway and diaphragm muscles induced by 5-HT1A receptor ligands. *Sleep & Breathing = Schlaf & Atmung*, **16**(1), 135–147.

Bianchi, A. L., Denavitsaubie, M., & Champagnat, J. (1995). Central control of breathing in mammals – Neuronal circuitry, membrane-properties, and neurotransmitters. *Physiological Reviews*, **75**(1), 1–45.

Butera, R. J., Rinzel, J., & Smith, J. C. (1999). Models of respiratory rhythm generation in the pre-Botzinger complex. I. Bursting pacemaker neurons. *Journal of Neurophysiology*, **82**(1), 382–397.

Dhingra, R. R., Dutschmann, M., & Dick, T. E. (2016). Blockade of dorsolateral pontine 5HT1A receptors destabilizes the respiratory rhythm in C57BL6/J wild-type mice. *Respiratory Physiology & Neurobiology*, **226**, 110–114.

Dutschmann, M., & Dick, T. E. (2012). Pontine mechanisms of respiratory control. *Comprehensive Physiology*, **2**(4), 2443–2469.

Dutschmann, M., & Herbert, H. (2006). The Kolliker-Fuse nucleus gates the postinspiratory phase of the respiratory cycle to control inspiratory off-switch and upper airway resistance in rat. *European Journal of Neuroscience*, **24**(4), 1071–1084.

Ermentrout, B. (2002). *Simulating, analyzing, and animating dynamical systems: A guide to XPPAUT for researchers and students* (vol. **14**). SIAM.

Ezure, K., Tanaka, I., & Saito, Y. (2003). Brainstem and spinal projections of augmenting expiratory neurons in the rat. *Neuroscience Research*, **45**(1), 41–51.

Flor, K. C., Barnett, W. H., Karlen-Amarante, M., Molkov, Y. I., & Zoccal, D. B. (2020). Inhibitory control of active expiration by the Botzinger complex in rats. *The Journal of Physiology*, **598**(21), 4969–4994.

Fung, M. L., & St John, W. M. (1995). The functional expression of a pontine pneumotaxic centre in neonatal rats. *The Journal of Physiology*, **489**(Pt 2), 579–591.

Gaytan, S. P., Calero, F., Nunez-Abades, P. A., Morillo, A. M., & Pasaro, R. (1997). Pontomedullary efferent projections of the ventral respiratory neuronal subsets of the rat. *Brain Research Bulletin*, **42**(4), 323–334.

Geerling, J. C., Yokota, S., Rukhadze, I., Roe, D., & Chamberlin, N. L. (2017). Kolliker-Fuse GABAergic and glutamatergic neurons project to distinct targets. *Journal of Comparative Neurology*, **525**(8), 1844–1860.

Hayward, L. F., Castellanos, M., & Davenport, P. W. (2004). Parabrachial neurons mediate dorsal periaqueductal gray evoked respiratory responses in the rat. *Journal of Applied Physiology*, **96**(3), 1146–1154.

Jakus, J., Poliacek, I., Halasova, E., Murin, P., Knocikova, J., Tomori, Z., & Bolser, D. C. (2008). Brainstem circuitry of tracheal-bronchial cough: c-fos study in anesthetized cats. *Respiratory Physiology & Neurobiology*, **160**(3), 289–300.

Jenkin, S. E., Milsom, W. K., & Zoccal, D. B. (2017). The Kolliker-Fuse nucleus acts as a timekeeper for late-expiratory abdominal activity. *Neuroscience*, **348**, 63–72.

Koolen, L. A. E. (2021). *Effects of serotonin 1A receptor transmission on neural control of respiration*. University of Bristol.

Kubin, L., Alheid, G. F., Zuperku, E. J., & McCrimmon, D. R. (2006). Central pathways of pulmonary and lower airway vagal afferents. *Journal of Applied Physiology*, **101**(2), 618–627.

Levitt, E. S., Hunnicutt, B. J., Knopp, S. J., Williams, J. T., & Bissonnette, J. M. (2013). A selective 5-HT1a receptor agonist improves respiration in a mouse model of Rett syndrome. *Journal of Applied Physiology*, **115**(11), 1626–1633.

Lindsey, B. G., Rybak, I. A., & Smith, J. C. (2012). Computational models and emergent properties of respiratory neural networks. *Comprehensive Physiology*, **2**(3), 1619–1670.

Manzke, T., Niebert, M., Koch, U. R., Caley, A., Vogelgesang, S., Hulsmann, S., Ponimaskin, E., Muller, U., Smart, T. G., Harvey, R. J., & Richter, D. W. (2010). Serotonin receptor 1A-modulated phosphorylation of glycine receptor alpha3 controls breathing in mice. *Journal of Clinical Investigation*, **120**(11), 4118–4128.

Molkov, Y. I., Abdala, A. P., Bacak, B. J., Smith, J. C., Paton, J. F., & Rybak, I. A. (2010). Late-expiratory activity: Emergence and interactions with the respiratory CpG. *Journal of Neurophysiology*, **104**(5), 2713–2729.

Molkov, Y. I., Bacak, B. J., Dick, T. E., & Rybak, I. A. (2013). Control of breathing by interacting pontine and pulmonary feedback loops. *Frontiers in Neural Circuits*, **7**, 16.

Molkov, Y. I., Rubin, J. E., Rybak, I. A., & Smith, J. C. (2017). Computational models of the neural control of breathing. *Wiley Interdisciplinary Reviews: Systems Biology and Medicine*, **9**(2), https://doi.org/10.1002/wsbm.1371

Molkov, Y. I., Shevtsova, N. A., Park, C., Ben-Tal, A., Smith, J. C., Rubin, J. E., & Rybak, I. A. (2014). A closed-loop model of the respiratory system: Focus on hypercapnia and active expiration. *PLoS ONE*, **9**(10), e109894.

Montalbano, A., Corradetti, R., & Mlinar, B. (2015). Pharmacological characterization of 5-HT1A autoreceptor-coupled GIRK channels in rat dorsal raphe 5-HT neurons. *PLoS ONE*, **10**(10), e0140369.

Morschel, M., & Dutschmann, M. (2009). Pontine respiratory activity involved in inspiratory/expiratory phase transition. *Philosophical Transactions of the Royal Society of London Series B, Biological Sciences*, **364**(1529), 2517–2526.

Occhipinti, R., Puchowicz, M. A., LaManna, J. C., Somersalo, E., & Calvetti, D. (2007). Statistical analysis of metabolic pathways of brain metabolism at steady state. *Annals of Biomedical Engineering*, **35**(6), 886–902.

Occhipinti, R., Somersalo, E., & Calvetti, D. (2010). Energetics of inhibition: Insights with a computational model of the human GABAergic neuron-astrocyte cellular complex. *Journal of Cerebral Blood Flow and Metabolism*, **30**(11), 1834–1846.

Occhipinti, R., Somersalo, E., & Calvetti, D. (2011). Interpretation of NMR spectroscopy human brain data with a multi-compartment computational model of cerebral metabolism. *Advances in Experimental Medicine and Biology*, **701**, 249–254.

Oku, Y., & Dick, T. E. (1992). Phase resetting of the respiratory cycle before and after unilateral pontine lesion in cat. *Journal of Applied Physiology*, **72**(2), 721–730.

Otake, K., Ezure, K., Lipski, J., & Wong She, R. B. (1992). Projections from the commissural subnucleus of the nucleus of the solitary tract: An anterograde tracing study in the cat. *Journal of Comparative Neurology*, **324**(3), 365–378.

Pagliardini, S., Janczewski, W. A., Tan, W., Dickson, C. T., Deisseroth, K., & Feldman, J. L. (2011). Active expiration induced by excitation of ventral medulla in adult anesthetized rats. *Journal of Neuroscience*, **31**(8), 2895–2905.

Phillips, R. S., & Rubin, J. E. (2022). Putting the theory into 'burstlet theory' with a biophysical model of burstlets and bursts in the respiratory preBotzinger complex. *Elife*, **11**, e75713.
Rubin, J. E., Bacak, B. J., Molkov, Y. I., Shevtsova, N. A., Smith, J. C., & Rybak, I. A. (2011). Interacting oscillations in neural control of breathing: Modeling and qualitative analysis. *Journal of Computational Neuroscience*, **30**(3), 607–632.
Rubin, J. E., Shevtsova, N. A., Ermentrout, G. B., Smith, J. C., & Rybak, I. A. (2009). Multiple rhythmic states in a model of the respiratory central pattern generator. *Journal of Neurophysiology*, **101**(4), 2146–2165.
Shevtsova, N. A., Manzke, T., Molkov, Y. I., Bischoff, A., Smith, J. C., Rybak, I. A., & Richter, D. W. (2011). Computational modelling of 5-HT receptor-mediated reorganization of the brainstem respiratory network. *European Journal of Neuroscience*, **34**(8), 1276–1291.
Silva, J. N., Lucena, E. V., Silva, T. M., Damasceno, R. S., Takakura, A. C., & Moreira, T. S. (2016). Inhibition of the pontine Kolliker-Fuse nucleus reduces genioglossal activity elicited by stimulation of the retrotrapezoid chemoreceptor neurons. *Neuroscience*, **328**, 9–21.
Smith, J. C., Abdala, A. P., Koizumi, H., Rybak, I. A., & Paton, J. F. (2007). Spatial and functional architecture of the mammalian brain stem respiratory network: A hierarchy of three oscillatory mechanisms. *Journal of Neurophysiology*, **98**(6), 3370–3387.
Stettner, G. M., Huppke, P., Brendel, C., Richter, D. W., Gartner, J., & Dutschmann, M. (2007). Breathing dysfunctions associated with impaired control of post-inspiratory activity in Mecp2-/y knockout mice. *The Journal of Physiology*, **579**(Pt 3), 863–876.
Takagi, K., & Nakayama, T. (1958). Respiratory discharge of the pons. *Science*, **128**(3333), 1206.
Varga, A. G., Maletz, S. N., Bateman, J. T., Reid, B. T., & Levitt, E. S. (2021). Neurochemistry of the Kolliker-Fuse nucleus from a respiratory perspective. *Journal of Neurochemistry*, **156**(1), 16–37.
Voituron, N., Menuet, C., Dutschmann, M., & Hilaire, G. (2010). Physiological definition of upper airway obstructions in mouse model for Rett syndrome. *Respiratory Physiology & Neurobiology*, **173**(2), 146–156.
Wittman, S., Abdala, A. P., & Rubin, J. E. (2019). Reduced computational modelling of Kolliker-Fuse contributions to breathing patterns in Rett syndrome. *The Journal of Physiology*, **597**(10), 2651–2672.
Zoccal, D. B., Silva, J. N., Barnett, W. H., Lemes, E. V., Falquetto, B., Colombari, E., Molkov, Y. I., Moreira, T. S., & Takakura, A. C. (2018). Interaction between the retrotrapezoid nucleus and the parafacial respiratory group to regulate active expiration and sympathetic activity in rats. *American Journal of Physiology. Lung Cellular and Molecular Physiology*, **315**(5), L891–L909.

Additional information

Data availability statement

The model code is available in the ModelDB repository (https://modeldb.science/2014996).

Competing interests

None of the authors has any conflicts of interests.

Author contributions

S.J. and W.B. generated and analysed data and drafted/revised the work; D.Z. and A.A. contributed to the conception of the work and revised the manuscript critically for important intellectual content; J.R. and Y.M. conceptualized and designed the work, analysed and interpreted data and drafted/revised the work. All authors approved the final version of the manuscript. All authors agree to be accountable for all aspects of the work in ensuring that questions related to the accuracy or integrity of any part of the work are appropriately investigated and resolved. All persons designated as authors qualify for authorship, and all those who qualify for authorship are listed.

Funding

This work was supported by Georgia State University Brains & Behaviour Seed Grant to Y.M., by the National Council for Scientific and Technological Development (CNPq) grant no. 303481/2021-8 and São Paulo State Research Foundation (FAPESP) grant no. 2022/05717-0 to D.Z., NSF DMS grant no. 1951095 to J.R. and NIH NCCIH grant no. R01AT008632 to Y.M., A.A and D.Z.

Keywords

control of breathing, Kölliker–Fuse, modelling, Rett syndrome

Supporting information

Additional supporting information can be found online in the Supporting Information section at the end of the HTML view of the article. Supporting information files available:

Peer Review History